Comparative Analysis of Performance and Mechanisms of Flood Inundation Map Generation using Height Above Nearest Drainage

Zhouyayan Li [a,b*], Felipe Quintero Duque[b], Trevor Grout[c,d], Bradford Bates[c,d], Ibrahim Demir [a,b]

[a] Dept. of Civil and Environmental Engineering, University of Iowa, Iowa City, Iowa, USA
[b] IIHR Hydroscience and Engineering, University of Iowa, Iowa City, Iowa, USA
[c] National Water Center, Tuscaloosa, Alabama, USA
[d] Lynker, Leesburg, Virginia, USA

* Corresponding Author, Email: zhouyayan-li@uiowa.edu

Abstract
For flood inundation extent prediction, it is important to have a faster, more accurate, and input-parsimonious model during response and recovery efforts. Height Above Nearest Drainage (HAND) is a simplified conceptual model whose efficacy and utility have been demonstrated in previous studies. This study aims to provide a comprehensive assessment of prediction performance of the rating-curve-based HAND generated with the framework adopted at NOAA's National Water Center and the non-rating-curve-based HAND inundation maps created with a web-based flood inundation mapping system. The study presents an in-depth analysis on the performance of HAND with varying model configurations, conditions where the HAND fails to provide accurate predictions, and underlying mechanism and guideline to overcome these challenges. The study also includes analysis of the model performance with bathymetry-based measurements. The results show that in areas where the water depth indicated by the synthetic rating curve are relatively consistent with those in catchments, the non-rating-curve-based HAND can generate comparable inundation extent predictions with fewer inputs. Otherwise, the non-rating-curve-based HAND may result in significant underestimations due to a combination of factors. The underestimation can be reduced by using a multi-depth technique to calculate water depth. Furthermore, the results show that the optimal HAND threshold is a percentage ranging between 8% and 12% of the basin drainage area, rather than a specific number as reported in previous studies. In comparison to the single-depth approach, the results show that proposed multi-point water depth calculation approaches are more robust against the causes of underestimation. However, there are no notable differences in prediction performance between proposed multi-point approaches. Finally, bathymetry measurements cause underestimation by increasing HAND values for non-drainage pixels. As a result, they should be handled with caution, as underestimation is riskier than overestimation when it comes to flood preparedness.

Keyword: Height Above Nearest Drainage; rating-curve-based HAND; non-rating-curve-based HAND; model configuration; performance analysis.

---

1. Introduction

Humans have been fighting against floods for centuries (Di Baldassarre *et al.* 2017, Ghosh and Kar 2018, de Lange 2019, Blöschl *et al.* 2020). Different from many other natural hazards, floods are reactions to a combination of natural and anthropogenic causes (Munoz *et al.* 2018, Bentivenga *et al.* 2020, Nicholls *et al.* 2021). Paved roads and poorly designed urban pipeline networks can disrupt the drainage process and exacerbate urban flooding (Lancia *et al.* 2020, Sun *et al.* 2021). Levee and dam breach and inappropriate reservoir operation during heavy precipitation and flooding events can bring unexpected inundation to unprepared communities and cause massive direct (Tadesse and Fröhle 2020, Yildirim and Demir 2021) and indirect losses (Psomiadis *et al.* 2021, Alabbad *et al.* 2022). Rapid landscape transformation in both rural and urban areas, combined with climate change is weeding our previous efforts to understanding and identifying (Haltas *et al.* 2021) and mapping flood events over the last few decades (Leitner *et al.* 2020, S Chegwidden *et al.* 2020, Abdrabo *et al.* 2022).

One possible solution to cope with the fast pace at which the physical world is changing is to integrate forecasts of factors that affect the magnitude and pattern of floods, such as conducting flood modeling based on precipitation (Chegwidden *et al.* 2020, Janizadeh *et al.* 2021), utilizing new precipitation data set collected in real-time (Seo *et al.* 2019) taking advantage of evaporation (Le and Bae, 2020) obtained from general circulation models (GCMs) and based on potential landcover schemes (Leitner *et al.* 2020, Janizadeh *et al.* 2021). Another viable option is to create and use fast modeling frameworks that are data-parsimonious, robust, and computationally efficient based on web technologies (Sit *et al.* 2019, 2021, Xu *et al.* 2019, Agliamzanov *et al.* 2020)

Currently, lack of benchmark datasets (Ebert-Uphoff *et al.* 2017) and large data requirements, such as channel profile, initial and side flows, and boundary conditions, is a major reason why many previously developed hydrodynamic modeling frameworks cannot be quickly applied to a new scenario (Savage *et al.* 2016, Teng *et al.* 2017), as many of those rely on on-site measurements or land surveys and often cannot be easily obtained or updated in a timely manner (Musser *et al.* 2016, McGrath *et al.* 2018). Robustness is another shortcoming of many existing physics-based modeling frameworks. For example, many hydrodynamic computations are extremely sensitive to Manning's roughness (Terezinha *et al.* 2017) which is an empirical coefficient whose initial value is usually obtained from tables, field surveys, and empirical formulas (Papaioannou *et al.* 2017). Calibration is always required to obtain the ideal roughness value that yields the best simulation result for any study region (Papaioannou *et al.* 2017, Garrote *et al.* 2021). As Manning's *n* is mostly governed by the physical characteristics of the channel (Nohani 2019), the coefficient value is particularly sensitive to common channel alterations, such as vegetation growth and dredging. Another important criterion to consider when selecting a model is computing efficiency, as time is of the essence, especially when getting prepared for floods. It is preferable to use models that produce accurate findings fast rather than models that produce precise results but take hours or even days to run.

Within the last decade, simplified-conceptual models have seen rapid growth and applications in flood inundation mapping. Due to their model structures, data and computational needs, these models ensure a better balance between the accuracy and speed. Many of these models are topography-based techniques that require a digital elevation model (DEM) or digital terrain model (DTM) as the primary input and only have a few parameters to adjust (Nardi *et al.* 2019, Baldassarre *et al.* 2020) as they do not generally solve hydraulic equations or require

initial and boundary conditions for calculation. These models can potentially benefit from DEM products of super resolution algorithms (Demiray *et al.* 2021) in the future.

Among all the simplified models, the Height Above Nearest Drainage (HAND) has been widely used for flood inundation extent prediction (Afshari *et al.* 2018, McGrath *et al.* 2018, Speckhann *et al.* 2018, Godbout *et al.* 2019, Jafarzadegan and Merwade 2019) because it produces comparable results to those produced by more complex modeling frameworks, such as the U.S. Army Corps of Engineers Hydrologic Engineering Center River Analysis System (HEC-RAS) (Afshari *et al.* 2018, Zheng *et al.* 2018, Li *et al.* 2022). A HAND-based inundation extent map is created by a pixel-by-pixel comparison between a particular water depth with the HAND value, which is the elevation difference between the present pixel and the pixel in drainage networks to which it drains (Nobre *et al.* 2011). For a detailed introduction to the HAND model, see section 3.1. In addition, the HAND model has been adopted for many other research purposes such as uncertainty analysis (Jafarzadegan and Merwade 2019, Michael Johnson *et al.* 2019) and reach-averaged rating curve generation (Zheng *et al.* 2018). Moreover, rather than simply applying the framework for analysis and comparison, several studies have been conducted to improve the framework's accuracy (Zheng *et al.* 2018, Shastry *et al.* 2019) and computational efficiency (Liu *et al.* 2018).

In the United States, the National Water Center (NWC) of the National Oceanic and Atmospheric Administration (NOAA) has developed a version of HAND to satisfy its nationwide directive to provide flood forecasting intelligence to American states and some territories. This implementation of HAND applies streamflow estimates from the National Water Model (NWM) to a HAND model to generate national-scale inundation maps. The NWC framework interpolates stage values from the NWM streamflow predictions using a synthetic rating curve that is unique to each catchment in the network. The stage is then converted to water depth and compared to the HAND values at the catchment-level (Maidment, 2017), thus providing a unique approximation of inundation for all catchments in the network. This entire approach is considered rating-curve-based because it is designed to use rating curves to interpolate stage values from streamflow values, however NWC HAND grid can be used independently of the NWM and rating curves, provided that stage values are available.

By contrast, many studies simply employed water depth measurements at hydrometric stations (McGrath *et al.* 2018) or on-site observations (Nobre *et al.* 2016) instead of translating streamflow to a stage and then to a water depth. This method will be referred to as the non-rating-curve-based HAND henceforth. The phrase "non-rating-curve-based" merely denotes that this framework does not generate its own rating curve for a study area; nevertheless, this does not preclude it from using stage estimates from existing rating curves to obtain depth value. Recently, HAND model is used to develop a client-side web-based inundation mapping system by (Hu and Demir 2021) taking advantage of the low data requirements and high computing efficiency of the non-rating-curve-based-HAND. The system can generate flexible inundation maps in real time with any given DEM, water depth, and the drainage threshold on standard personal computers.

Because river stage values are not available for every stream in the US domain, it is necessary for the National Water Center HAND (herein referred to as NCWH) to use rating curves to interpolate stage values for all rivers using NWM streamflow values, which are available at nearly 3 million streams. For this reason, the NWCH inundation product has additional data dependencies and requires additional compute resources in order to perform flow to stage interpolations. However, if stage values were available for the entire US and its

territories, then the NWCH rating curves would no longer be necessary. As mentioned above, the NWCH rating curve is derived from hydrologic modeling that involves solving Manning's equation. Also, the NWCH method for calculating inundation extent at the reach-catchment level (Maidment 2017) requires additional data such as the NWM stream network and catchment geometry files, which are relatively static. In addition, because the NWCH implementation of HAND was custom designed for the United Stated domain, it is not immediately applicable to regions outside of the United States where the data dependencies are not always available or in an acceptable format.

By contrast, the non-rating-curve-based approach needs only the DEM data and a water depth value as the input which allows great flexibility and potential for this approach to be applied anywhere in the world, if water depth information is available. However, currently we lack a detailed comparison between these two approaches to ensure us the simpler one can generate comparable results. Also, in cases where the simpler method fails to bring satisfying results, it is necessary to know how we can improve the performance without increasing model complexity and data requirement too much. In addition, currently, we still lack in-depth understanding of the mechanism of HAND, such as how the performance varies with different model configurations; why and when HAND model fails to give satisfying inundation extent predictions; is it possible and how we could further improve the performance of HAND; and how the performance will change with additional terrain information such as bathymetry measurements?

This study aims to address the following research challenges a) the performance of the non-rating-curve-based HAND compared to results from rating-curve-based one, b) analyzing mechanisms and impact on the performance of HAND with different model configurations and computing processes and come up with methods for model performance improvement; and c) investigating impacts of bathymetry information on model performance. The study summarizes the results with general guidelines on HAND model setup and performance enhancements aiming at providing an in-depth analysis of the HAND's performance as well as some universal results and implementation recommendations to help local communities, stakeholders, and decision-makers (Ewing and Demir 2021).

2. Study Area and Data Collection
The sub-watersheds that encompass the cities of Clarksville and Rock Valley, Iowa are selected as the area of study. The region for Clarksville study consists of two HUC 12 sub-watersheds, #070802020704 and #070802020701, that together cover 145 km^2 and have a total stream length of 112 km. The study region for Rock Valley is included in the HUC 12 sub-watershed #101720240804 with a drainage area of 105 km^2 and a total stream length of 66 km. The study area is depicted in Figure 1. These two study areas will be referred to as Clarksville and Rock Valley for the sake of simplicity. This simply indicates that the study areas are located near these two cities and does not imply that we are studying urban flooding in this paper. The sub-watersheds are chosen considering data availability and computational efficiency.

2.1. Reference Flood Inundation Maps and Comparison Scope
This research compares and analyzes inundation extents from two HAND model frameworks, NWCH and the non-rating-curve-based HAND, as well as HEC-RAS simulations for the same scope. The HEC-RAS simulations benefit from the Iowa Flood Center's (IFC) statewide floodplain mapping effort (Gilles *et al.* 2012) and will be used as reference flood maps for

validation. These consist of a collection of inundation maps corresponding to a series of stage values separated by 0.5 foot. These detailed inundation maps at the local scale have been integrated into the Iowa Flood Information System (IFIS).
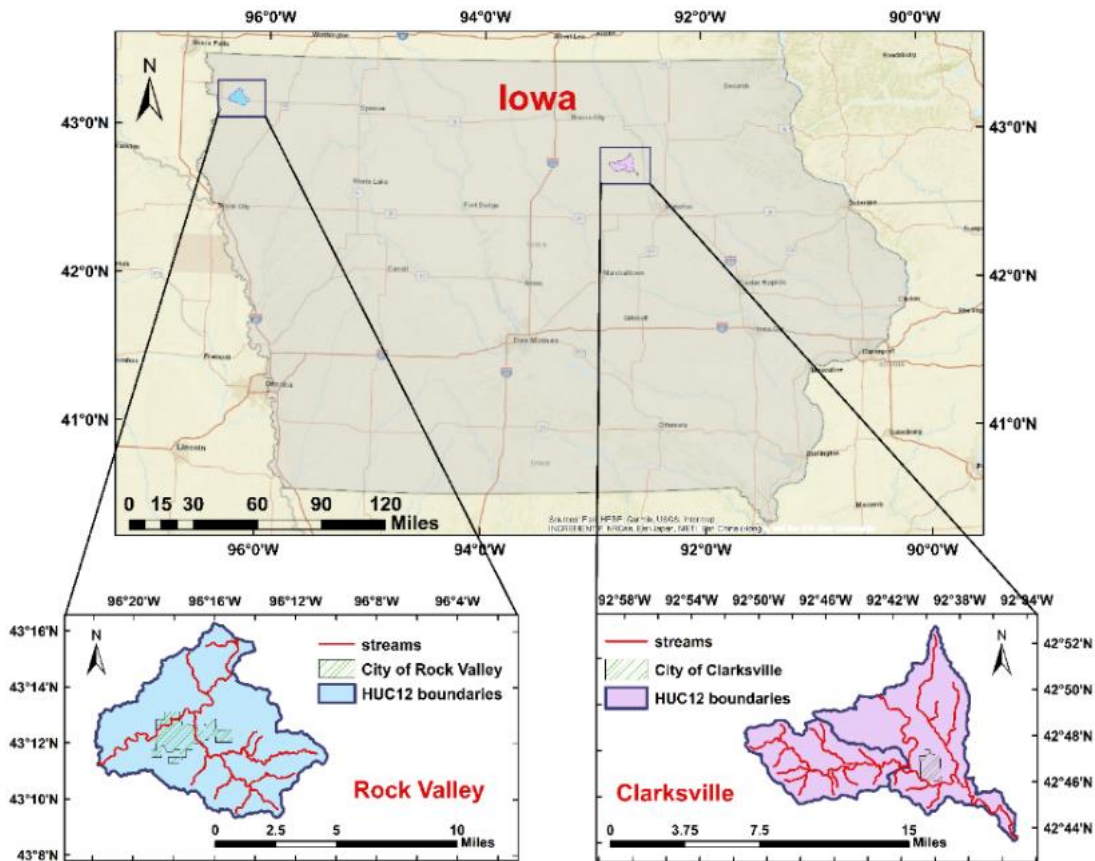
Figure 1. Location of the combined sub-watersheds #070802020704 and #070802020701, which contain the City of Clarksville, and the sub-watershed #101720240804, which contains the City of Rock Valley, Iowa

The NWCH inundation extent maps are the result of simulations run at the National Water Center with FIM 3.0.9.0 fr. Those maps are developed specifically for this study at the National Water Center. The non-rating-curve-based HAND inundation maps are generated using the web-based flood inundation mapping system developed by Hu and Demir (2021) and enhanced by (Li and Demir 2022) (see subsection 2.3 for a brief introduction on the system) and will be referred to as WBH hereinafter. The NWCH was run for the entire HUC 8 watersheds Rock (#10170204), and Shell Rock (#07080202), and the inundation extent was provided within a mask. Figure 2 shows the actual analysis (calculation) scope of WBH and evaluation (masks) areas for Rock Valley and Clarksville.

As illustrated in Figure 2, the actual area for which we are comparing the extent of inundation comprises several catchments in Rock Valley and Clarksville, respectively. There are two primary reasons for using a restricted area for comparison and analysis. The first is that the NHDPlus dataset contains about 2.7 million catchments for the continental United States. They each averages a surface area of 3 km^2 and a length of 2 km and is traversed by a single flow line

(Maidment 2017). Those catchments are the smallest units the simulation of NWCH runs on. The area and stream length of each catchment are listed in Table 1.
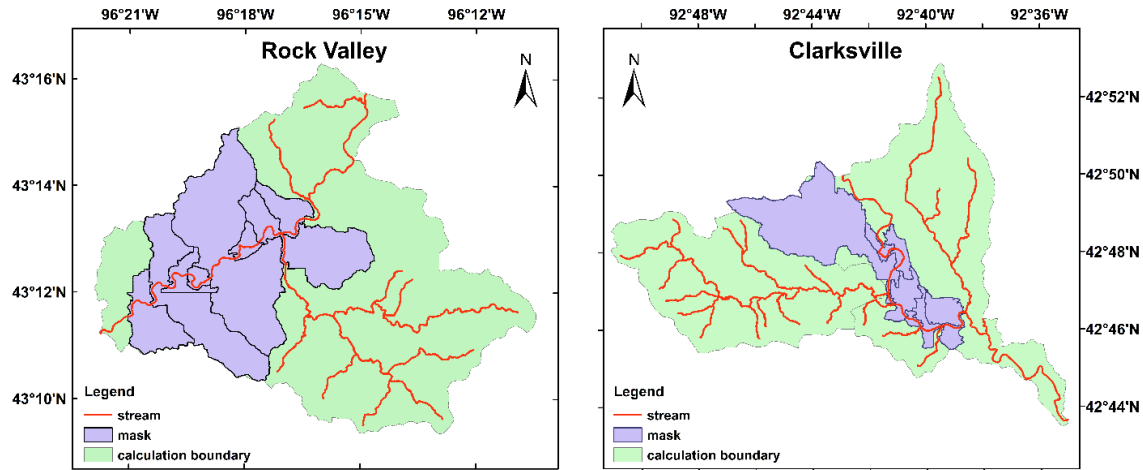
Figure 2. Location of catchments in which we compare flood inundation extent from NWCH, WBH, and the reference maps for Rock Valley (a) and for Clarksville (b)

Table 1. Summary of terrain characteristics of the catchments in Rock Valley and Clarksville

Rock Valley				Clarksville			
HydroID	Area (km²)	Median Thalweg Elevation (m)	length (m)	HydroID	Area (km²)	Median Thalweg Elevation (m)	length (m)
21110025	7.75	370.86	1434	17450065	0.92	281.39	1461
21110023	0.52	372.28	1437	17450066	1.54	280.51	1465
21110021	0.76	373.78	1436	17450067	18.50	280.14	1414
21110022	15.29	372.87	1438	17450060	0.13	279.94	634
21110024	1.13	371.37	1437	17450058	2.44	279.73	1013
21110029	1.74	375.81	1350	17450059	0.41	279.50	996
21110026	3.41	369.97	1440	17450057	1.38	278.37	1126
21110020	1.46	374.77	1442	17450055	1.01	278.30	1073
21110866	5.10	377.15	1272	17450056	2.25	278.06	1046

Another reason is that detailed reference flood extent maps are only available in the vicinity of some Iowa cities. Therefore, we confine our analysis to areas surrounding the two study cities. We chose reference flood inundation maps of 50-, 100-, and 500-year floods scenarios in Rock Valley and used the inundation extent for stages 18.0, 19.0, and 20.5 feet in Clarksville as the corresponding discharges are close to the estimates of the return period scenarios (50-, 100-, and 500-year floods). To keep things simple, we will continue to refer to them as the 50-, 100-, and 500-year scenarios.

2.2. Data Requirements for Rating-Curve-Based NWCH Inundation Maps
The National Water Center leverages datasets produced by the NWCH version 3.0 technique (NOAA 2021) to fulfill its directive to provide national inundation predictions. The datasets required for this task include HAND grids (full-resolution and mainstem configurations),

synthetic rating curves (full-resolution and mainstem configurations), model network cross-walking information (full-resolution and mainstem configurations), a representation of the HAND-derived catchments (full resolution and mainstem configurations), and catchment-specific flow values. The flow values can be supplied to the model by a river discharge model, such as the National Water Model (NWM), or from historic observations or other sources (i.e., crowdsourcing).

NWCH 3.0 uses two configurations, full-resolution and mainstem. The full-resolution configuration's stream network resembles that of the NWM. The mainstem configuration resembles only the stream segments that are downstream of an official Advanced Hydrologic Forecasting Service (AHPS) forecast site. NWCH 3.0 uses a mainstem configuration to better represent inundation in higher-order streams, whereas the full-resolution configuration is subject to underprediction of inundation extent in higher-order streams, primarily because of artificial restriction of inundation by catchment boundaries. The NWCH implementation can be found at the GitHub repository of Flood Inundation Mapping for U.S. National Water Model (https://github.com/NOAA-OWP/inundation-mapping).

2.3. Data Requirements for Non-Rating-Curve-Based WBH Inundation Maps

We generated non-rating-curve-based inundation maps using a web-based real-time flood inundation mapping system created by Hu and Demir (2021). The system can provide on-demand inundation predictions and hydro-spatial analysis products utilizing both pre-stored and user-supplied datasets. With the necessary dataset, the system can work with a variety of different calculation methods, perform result comparison and hydro-spatial analysis, and perform flood mitigation tasks in any study region selected by the user (Li and Demir, 2022). As a result, it enables the performance testing of models with varied configurations for this study.

The amount of data required for the system to generate inundation maps depends on the products desired by users and the corresponding calculation procedures. Data and information utilized during the study includes DEM and river networks from NHDPlus dataset, LiDAR-based DEM, bathymetry data gathered during field measurements, synthetic rating curves derived from HEC-RAS simulations for the two study areas, reach-averaged rating curves and reach information (such as location, area, and stream length as specified in Table 1) from NWM simulations for reaches inside the two study areas depicted in Figure 2, and location and relevant information of the closest USGS gauges for the two study areas (#06483500 for Rock Valley and #05462000 for Clarksville).

To compare the performance of NWCH with the WBH, the DEM raster from the NHDPlus is clipped, translated to meters, and resampled to 10-m resolution. For sensitivity analysis with various model setups, the 1-m LiDAR-based DEM was resampled to 5-m resolution. The 10-m resolution was chosen to maintain consistency with the NWCH data, and the 5-m resolution was chosen to balance computing efficiency and accuracy for sensitivity analysis. To examine the effect of bathymetry information on the model's performance, we substituted the 5-m DEM value with bathymetry measurements for all pixels in the stream network.

It's worth noting that some of the items stated above are required simply because we're comparing our results to those from NWM and to maintain data consistency. Indeed, the WBH system is far more adaptable in terms of data requirements. For example, in this study, we need the rating curves to determine the stage for a specific discharge, but we can also feed a water depth measurement directly into the system. Similarly, while the river network and information

from USGS gauges aid in selecting the placement of outlet pixels in this study, the location of outlet pixels can be completely custom and without restrictions.

3. Methodology

3.1. HAND Model

Height Above Nearest Drainage (HAND) model is a quantitative terrain descriptor initially introduced by (Rennó *et al.* 2008). HAND values are the differences in elevation between each pixel on hillslope and the nearest point in the river network that drains it. Numerous studies have established that the HAND model accurately represents the soil water environment (Nobre *et al.* 2011). Generating the HAND model starts from removing spurious depressions and flats from the raw Digital Elevation Model (DEM) to make it hydrologically coherent (Rennó *et al.* 2008, Nobre *et al.* 2011). Then, the flow direction of each pixel on the DEM is calculated using one of the widely adopted algorithms, e.g., D_8 (Mark 1984), or D_∞ (Tarboton 1997).

Next, we calculate the accumulating area which is the total number of upstream pixels the current one drains. This process is carried out for each pixel on the DEM. By comparing the accumulating values with a predefined drainage threshold, we separate drainage points (dark-color grid cells in Figure 3c) from non-drainage ones. Then, we divide all non-drainage pixels into different sub-catchments based on which drainage point they drain to as shown in Figure 3c. Finally, the HAND value of each non-drainage pixel is obtained by subtracting the elevation of the nearest drainage pixel from its original elevation, which is also called elevation normalization. The HAND values for drainage pixels are set to zero meaning they do not have drainage potential as they are the lowest points within the drainage network. The final product or HAND model is a matrix of HAND values of the same numbers of column and row as the DEM processed. Figure 3 shows a graphic representation of the HAND procedure.
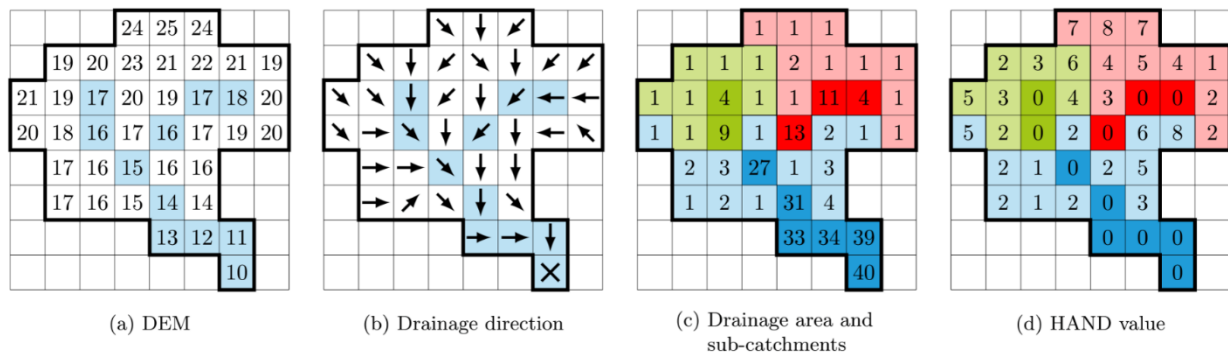
Figure 3. Major calculation steps of the HAND model. Figure reproduced from Rebolho *et al.* (2018)

3.2. NWCH Inundation Mapping

In the NWCH, each river segment is encoded with a "feature_id" and a discharge value. Because the NWCH-derived hydrologic network differs from the National Water Model network, model crosswalk information is needed to associate NWM discharge values with the HAND-derived catchments. After crosswalking the NWM discharge values to the NWCH catchments, catchment-specific synthetic rating curves are used to interpolate stage heights from the discharge values on a catchment-by-catchment basis. This interpolation results in a spatial array where values are encoded according to the catchment-specific interpolated stages. The HAND grid is then subtracted from this spatial array to derive inundation depths.

This process is performed for both the NWCH full-resolution and the mainstem configurations to generate two depth grids for the same area. A follow-up procedure is performed to mosaic the full-resolution and mainstem grids, prioritizing the maximum pixel value, i.e., maximum depth, when the same pixel location has a value provided by both configurations. Depending on the use-cases for the inundation information, the final mosaicked depth grid may be reclassified to a binary wet/dry inundation map and converted to a polygon.

For the purpose of this analysis, only the NWCH full-resolution configuration was used, i.e., not the full-resolution and mainstem composite inundation map.

3.3. WBH Inundation Mapping

WBH compares the HAND value of each pixel directly with depth values to decide the inundation extent. The stages may come from measurements at hydrometric stations, estimates obtained from rating curves, and crowd-sourced observations collected during flooding events on social media. In this study, the stage estimates for the entire study area and each catchment are obtained from the synthetic rating curve by HEC-RAS and the reach-averaged rating curves produced by the NWM simulations.

We developed four methods for calculating the inundation extents of the WBH including single depth the single depth (D_S), area-weighted depth (D_A), stream-length-weighted depth (D_L), and the local depth (D_{Local}) approaches. As implied by the name, D_S applies a single water-depth value to the entire study area. That water depth is calculated from the stage estimate using HEC-RAS synthetic rating curve at the USGS gauge location. The remaining three techniques make use of stage estimations derived from reach-averaged rating curves for each of the previously specified catchments. Rather than using a single-stage value, a few depths are applied to the model concurrently or participate in the derivation of the final depth value to be applied. For D_{Local}, multiple water depths are applied directly at the outlet of each catchment in the two study areas. While D_A and D_L calculate a single depth value by averaging all depths by reach area and stream length, respectively. The derived depth is then applied to the entire study area. In this study, we use Eq. 1 to calculate the water depth at a specific location.

$$depth = water\ stage + elevation\ of\ reference\ (\pm datum\ adjusting$$
$$factor) - elevation\ at\ the\ location\ the\ depth\ to\ be\ applied \qquad (Eq. 1)$$

In this calculation, datum adjusting factor allows us to convert the water elevation under the vertical datum for the reference point (normally NGVD29 for USGS gauges) to a datum that matches the DEM (NAVD88 in our case). The two USGS gauges serve as the reference points for D_S. Because there are no USGS gauges in each small catchment, we adopted the median elevation of thalweg of each reach as the elevation of references for the multi-depth ones (D_A, D_L, and D_{Local}). These elevation values have the same vertical datum as other DEM pixels and thus do not need datum conversion. After getting the stage estimates, corresponding water depths were calculated for the outlets of each catchment.

3.4. Performance Comparison between NWCH and WBH

The WBH inundation extent maps for 50-, 100-, and 500-year flooding scenarios were created and compared to corresponding reference extents and the NWCH extents. Here, we only use D_S for comparison to see if WBH can produce comparable results with the minimum data, namely, a DEM, a drainage threshold value without calibration, and a single water depth. The same 10-m

DEM used by the NWCH is fed into the WBH, which performs a series of automated processes to remove artificial pits and flats from the raw DEM and create a hydrologically coherent surface. The depth data was derived using Eq. 1 and the stage estimates from the synthetic rating curve. Eq. 1 and stage estimates from the synthetic rating curve were used to calculate the depth. For the drainage threshold, we assumed that no additional information or guidelines were available and thus chose 4.0 km^2 as previous studies had shown its efficacy (Nobre *et al.* 2016).

3.5. Sensitivity Analysis of the Performance of WBH

Model configurations with various drainage thresholds and depth values are computed and evaluated. The drainage threshold distinguishes pixels in main channels (also known as drainage pixels) from those on hillslopes (or called non-drainage pixels). As stated in subsection 3.1, drainage pixels have a HAND value of 0, and they are the points to which the elevation of non-drainage pixels is normalized. By changing the threshold value, we can modify the numbers of drainage pixels and thus modify the simulated network. In this study, the threshold being tested starts from 1 percent of the study area and increases by 1% each time until the model performance stabilizes. For each flooding scenario investigated in this study, D_S, D_A, D_L, and D_{Local} are computed and applied along with each threshold value, resulting in $e \times n \times (t_1 + t_2)$ different model configurations, where e is the numbers of flooding scenarios, n is the number of depth calculating approaches, and t_1 and t_2 and the number of tested threshold values in Rock Valley and Clarksville, respectively.

3.6. Investigating the Impact of Bathymetry Data

After we replace the elevation values in the stream networks with bathymetry measurements, changes will occur not only in model performance but also in how the performance pattern varies among model configurations. As a result, the previous sensitivity analysis results may not apply to the DEM with bathymetry information. With this in mind, we organized the bathymetry testing cases in the same way we did the sensitivity analysis, resulting in an additional $e \times n \times (t_1 + t_2)$ model configurations.

3.7. Evaluating Model Performance

A two-by-two contingency Matrix (Provost 1998) was used to categorize any pixel on a map's simulated inundation conditions into one of four classes: True-Positive (TP) means the pixel is predicted inundation by the model and indicated inundation on the reference map; True-Negative (TN) means the pixel is predicted dry by both the model and the reference; False-Positive (FP) means the pixel is predicted inundated by the model but is dry on the reference map; and False-Negative (FN) the pixel is predicted dry by the model but is actually inundated by the reference. The contingency matrix is depicted in Figure 4.

To further facilitate interpretation, we will compare the predicted extents with the reference visually and mathematically with the following indexes. Numerous indexes are available in the literature that can be used to evaluate model performance (Wilks 2011). To assess the agreement between the two maps, we used Proportion Correct, Bias, Hit Rate, Kappa value, and Fitness-statistic.

Proportion Correct (PC) has a value between 0 and 1, with 1 being the best. PC is a widely used index with the limitation of being unable to distinguish between FP and FN because they are treated equally in Eq. 2. It is calculated as follows:

$$PC = \frac{TP + TN}{TP + FN + FP + TN} \qquad\qquad (Eq.\,2)$$

Real Values

		Positive	Negative
Predicted Values	Positive	TP	FP
	Negative	FN	TN

Figure 4. The contingency matrix to indicate the inundation condition of any pixel on predicted maps and the reference map. Figure reproduced from Li *et al.* (2022)

Bias (B) is a positive value that with the best possible value of 1. B is not an accuracy measure (Wilks 2011) but indicates whether the scene is overestimated (B > 1) or underestimated (B < 1) in general. It is calculated as:

$$B = \frac{TP + FP}{TP + FN} \qquad\qquad (Eq.\,3)$$

Hit Rate (H) ranges between 0 and 1 with the best possible value of 1. H represents the ratio of inundated pixels on the reference maps that are captured by the predictions. H is also referred to as the Probability of Detection (POD), the true-positive fraction, and the sensitivity. (Wilks 2011). It is calculated as:

$$H = \frac{TP}{TP + FN} \qquad\qquad (Eq.\,4)$$

Kappa Value (K) can be negative, indicating that the prediction is worse than a random guess (Juurlink and Detsky 2005). The best value for K is 1. It is calculated as follows:

$$K = \frac{N(TP + TN) - \big((TP + FP) \times (TP + FN) + (FP + TN) \times (FN + TN)\big)}{N^2 - \big((TP + FP) \times (TP + FN) + (FP + TN) \times (FN + TN)\big)} \qquad (Eq.\,5)$$

Fitness Statistics (F), also known as Critical Success Index (CSI) (Wilks 2011), ranges between 0 to 1 with the best possible value of 1. It is calculated as:

$$F = \frac{TP}{TP + FN + FP} \qquad\qquad (Eq.\,6)$$

K and F complement each other. K focuses more on the dry pixels and are prone to bias when there are much more correctly predicted dry pixels than correctly predicted flooded pixels

(Afshari *et al.* 2018). Whereas F stresses more on the consistency of the flooded pixels on both maps.

4. Results and Discussion
4.1. Validating Rating Curves from HEC-RAS with USGS Estimates
The USGS rating curve for gauges near Rock Valley (06483500) and Clarksville (05462000) are plotted alongside the HEC-RAS estimations in Figure 5. The USGS rating curve is available through the USGS National Water Information System. The USGS estimates on these two sites have over a thousand stage-discharge pairs. The HEC-RAS, on the other hand, calculates discharge values for a stage series ranging from 8 to 25 feet for the Rock Valley community and from 9 to 20.5 feet for the Clarksville community, with a 0.5-foot interval for both. To facilitate comparisons between the two rating curves, the simulation points of HEC-RAS were connected on the graph.
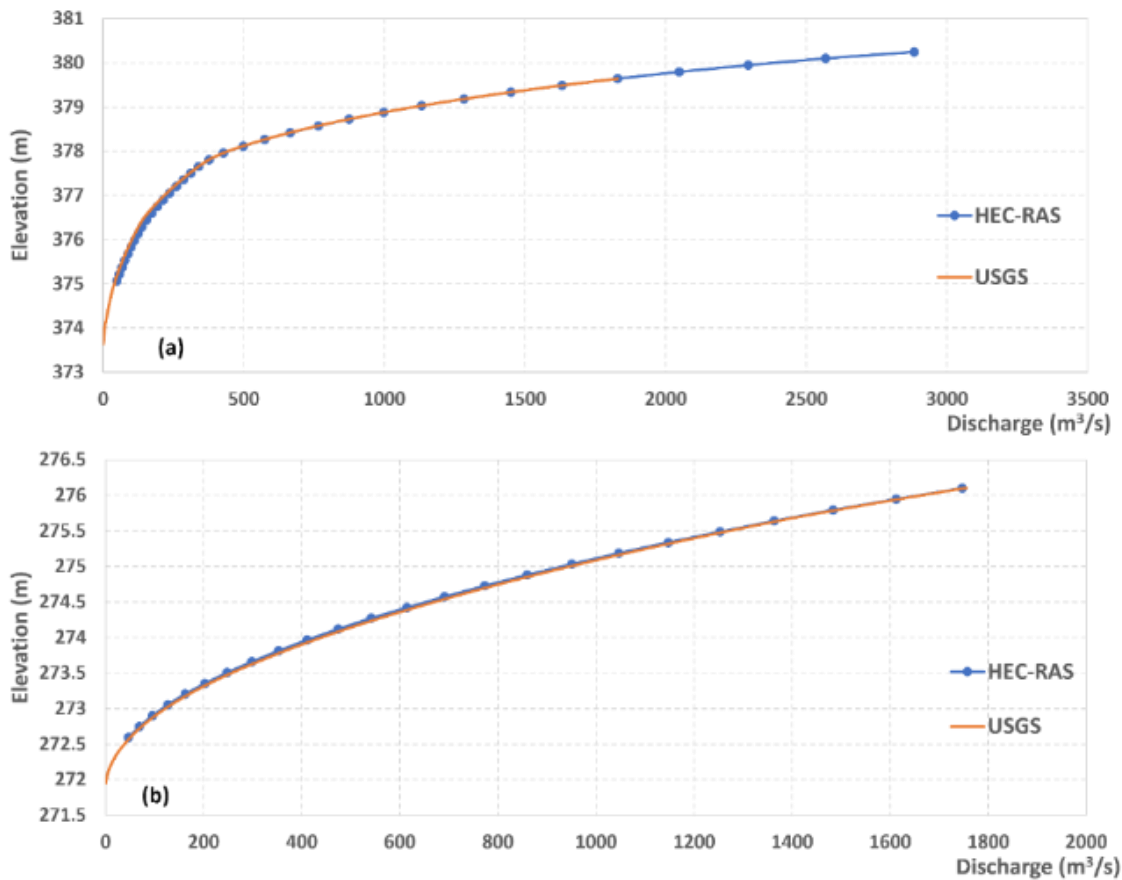
Figure 5. Synthetic rating curves for Rock Valley (a) and Clarksville (b), with USGS and HEC-RAS estimates plotted together

As illustrated in Figure 5, the estimated rating curves by HEC-RAS and the USGS are well aligned. This comparison is necessary because the reference floodplain maps are generated using HEC-RAS simulation. In addition, in order to calculate the corresponding water depth in this study, we need the streamflow or stage from HEC-RAS simulations. As a result, we must ensure that the HEC-RAS simulations match the USGS estimates.

4.2. Comparison of NWCH and WBH Flood Inundation Predictions

The results of the NWCH and WBH compared to the reference inundation extent for Rock Valley and Clarksville in 100- and 500-year flooding scenarios are shown in Figures 6 and 7. The top two sub-figures on both figures are comparisons of the WBH and the reference, while the bottom two are comparisons of the NWH and the reference. To show the locations, the transparency of the two (d) sub-figures is adjusted. Table 2 displays the prediction evaluating indexes in comparison to the reference.
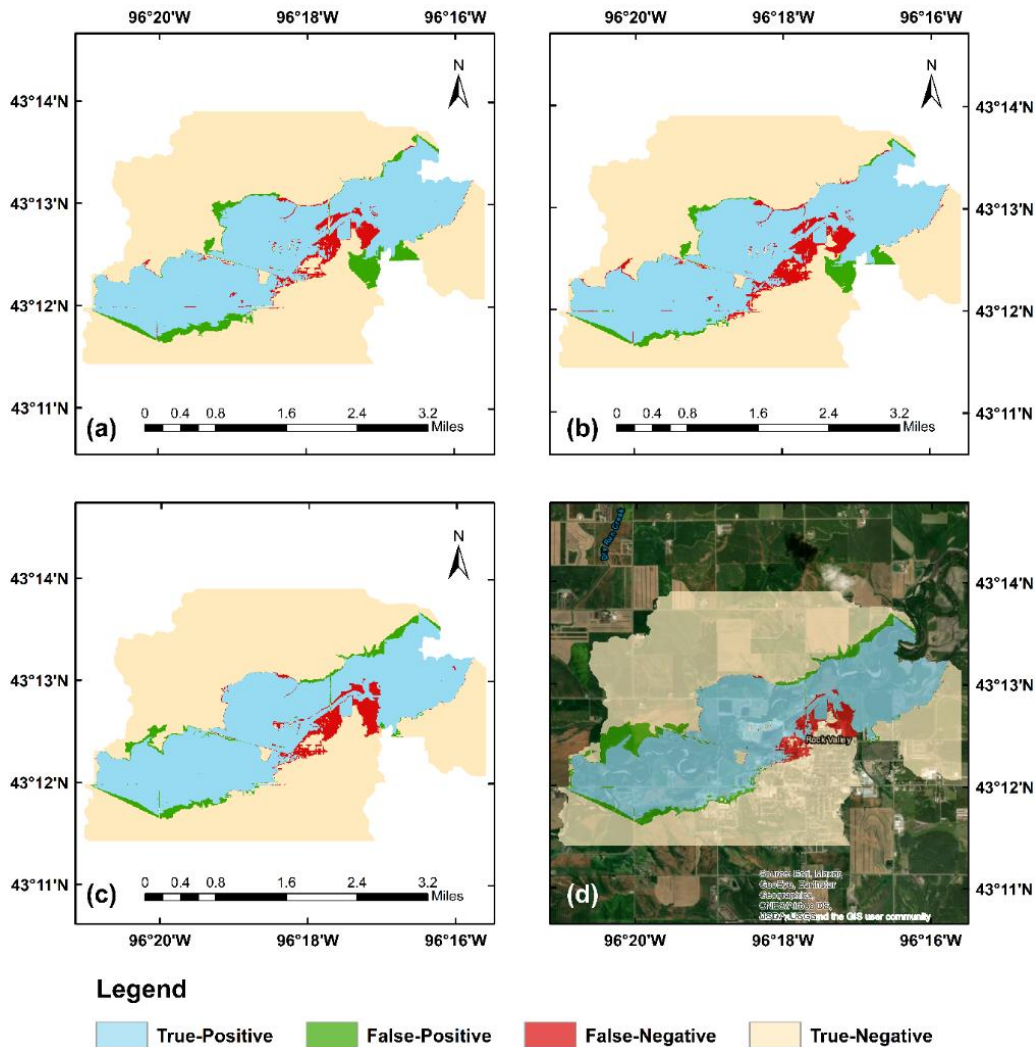
Figure 6. Predictions of inundation extent in Rock Valley compared to reference maps. The two sub-plots in the top row compare WBH to the reference in 100-year (left) and 500-year flood scenarios (right). The comparisons between the NWCH and the reference in 100- and 500-year scenarios (left to right) are shown in the bottom row.

When the False-Positive areas (in green) on 100-year predictions are compared to those on 500-year predictions in Figure 6, the WBH generates slightly less overestimation for the 500-year flooding scenario around the lower-left and upper-right corners but more underestimation (in red) in the middle of the map. When compared to the WBH, the NWCH predicts slightly more overestimation along the upper border of the inundation extent in both flooding scenarios

while producing less underestimation in the middle of the image in the 500-year one. According to the B index in Table 2, the predictions of the NWCH and WBH approaches for the 100-year flood are slightly underpredicted and overpredicted, respectively, and it is the opposite for the 500-year flood. Other indices show no significant difference in performance between the two modeling frameworks for both flooding events.

In Clarksville, the WBH with D_S failed to capture as many inundated pixels on the reference map as the NWCH does for both flooding events, as shown in Figure 7 by comparing (a) with (c) and comparing (b) with (d). On both banks of the main channel's central portion, there is significant underestimation on the WBH map (a and b). NWCH extents, on the other hand, are generally more accurate while being slightly overestimated for both events. In addition, the performance of NWCH in the 500-year scenario is more balanced in terms of the amount of over and underestimation than in the 100-year scenario, as shown in Table 2.
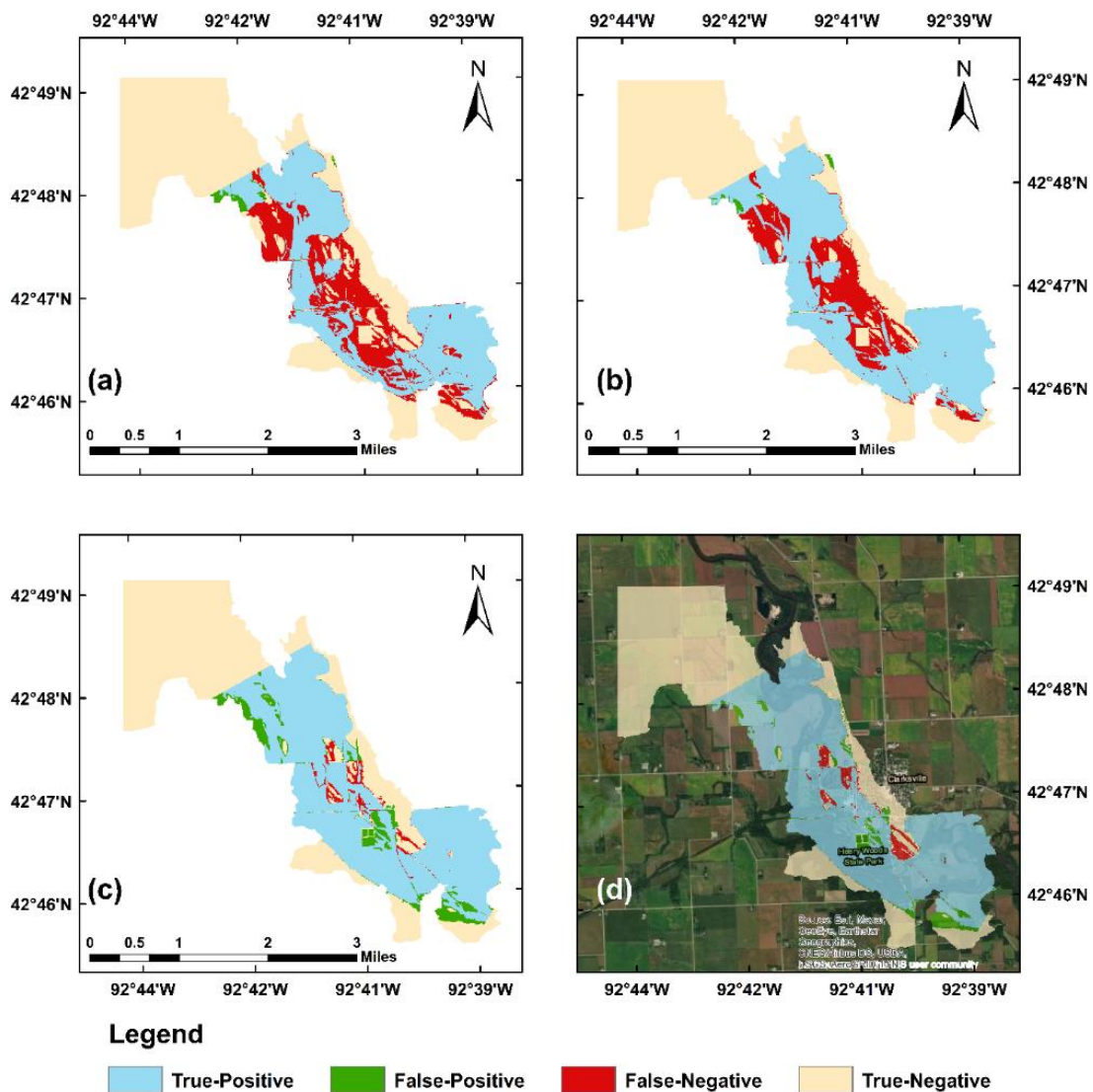
Figure 7. Predictions of inundation extent in Clarksville compared to reference maps. The two sub-plots in the top row compare WBH to the reference in 100-year (left) and 500-year flood

scenarios (right). The comparisons between the NWCH and the reference in 100- and 500-year scenarios (left to right) are shown in the second row of sub-plots.

Table 2. Numbers of pixels classified as True-Positive, False-Negative, False-Positive, and True-Negative when compared to reference maps and the corresponding evaluating indexes.

	flooding event	Threshold (km²)		TP (pixels)	FN (pixels)	FP (pixels)	TN (pixels)	FN+FP (pixels)	PC	B	H	K	F
Rock Valley	100-yr event	-	NWCH	80268	6770	6057	165209	12827	0.95	0.99	0.92	0.89	0.86
		4km²	WBH	81249	5789	9430	161836	15219	0.94	1.04	0.93	0.87	0.84
	500-yr event	-	NWCH	86779	5283	10648	155594	15931	0.94	1.06	0.94	0.87	0.84
		4km²	WBH	83449	8613	7230	159012	15843	0.94	0.98	0.91	0.87	0.84
Clarksville	100-yr event	-	NWCH	77954	2776	7869	73784	10645	0.93	1.06	0.97	0.87	0.88
		4km²	WBH	54117	26613	1170	80483	27783	0.83	0.68	0.67	0.66	0.66
	500-yr event	-	NWCH	83355	3243	5306	70479	8549	0.95	1.02	0.96	0.89	0.91
		4km²	WBH	65615	20983	755	75030	21738	0.87	0.77	0.76	0.74	0.75

The underestimation in WBH's prediction for Clarksville might be caused by three main factors: 1) input data resolution loss during data format conversion; 2) limitations in algorithm used for resolving flats, which results in elevation increase in specific locations; and 3) low values for depth derived from the synthetic rating curve.

There are two major factors that could influence the input data resolution loss during the calculation of the WBH system's HAND matrix including data format and conversion. Because TIFF is not a well-supported format for web applications, the DEM data is converted to an RGB PNG file from the original format of TIFF for use in the web-based system. The system must then convert the RGB values back to elevation values in order to perform a pixel-level computation. This two-way conversion might introduce uncertainty into the HAND matrix calculation. Furthermore, the system stores each pixel's HAND value in integer format. This is because the system is designed and optimized to run efficiently on standard personal computers. As a result, it makes use of the efficient built-in data structure of the programming language that is used to create the system. The system's core language, JavaScript, handles arrays of integers more efficiently than arrays of float numbers.

As mentioned in the previous section, HAND matrix generation is based on flow directions of pixels derived from a hydrologically coherent DEM after flats (due to both natural flats and pit-resolving algorithms) are removed. To resolve the imperfections on the DEM, the WBH system employs the algorithm proposed by (Barnes *et al.* 2014). This algorithm first detects flats, which consist of a cluster of nearby pixels with equal elevation values, and then raises the elevation of those pixels based on their distance from the surrounding non-flat pixels (referred to as *the gradient away from higher terrain*) and the outlet of the entire flat area (referred to as *the gradient towards lower terrain*). The algorithm increases the elevation of a pixel more if that pixel is closer to the non-flat surrounding pixels. Similarly, the further a pixel is away from the flat area's outlet, the greater the elevation increase will be. As a result, it ensures the generation of flow direction for each pixel at the expense of changing directions for some pixels for which the elevation values increase. In the upper box of Figure 8, the stream initially flows downward before merging with the mainstream to the right. However, as the segment's elevation rises, it flows upward, merges with the main channel, and disconnects the stream in between. Same reason also applies to the situation in the lower box but is less obvious. This is unavoidable for

flat resolving algorithms because they require elevation changes to force flows to drain from previously flat regions. As a result, the inundation condition and localized flow directions may differ from what the raw DEM indicates.
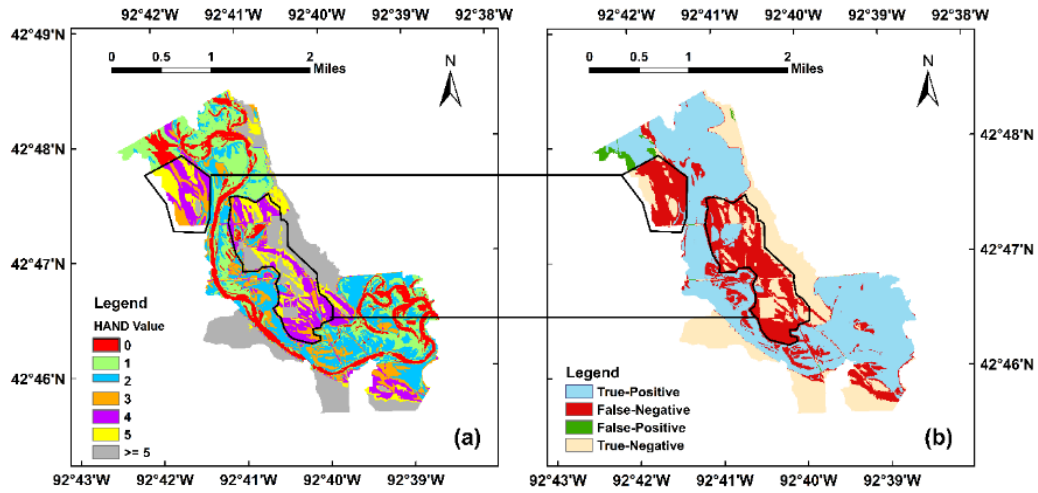
Figure 8. Predictions of flood inundation in a 100-year scenario (b) and visualization of the corresponding HAND matrix (a). The underestimation in the upper and lower black boxes is primarily due to elevation changes caused by the pit-removal algorithm and a small depth estimate derived from the synthetic rating curve.

Although the first two factors can cause some localized changes in the inundation condition, we believe that the last reason is the primary contributor to the underestimation in Clarksville because elevation increase occurred in only 4.8 percent of the pixels in the comparison. Approximately 77 percent of the pixels that were changed only had a one-meter elevation increase. Furthermore, the results in Rock Valley were generated using the same computation framework and algorithm but did not show significant underestimation compared to those from NWCH. The depth values derived from the synthetic rating curve and the corresponding depths in each catchment are shown in Figure 9.
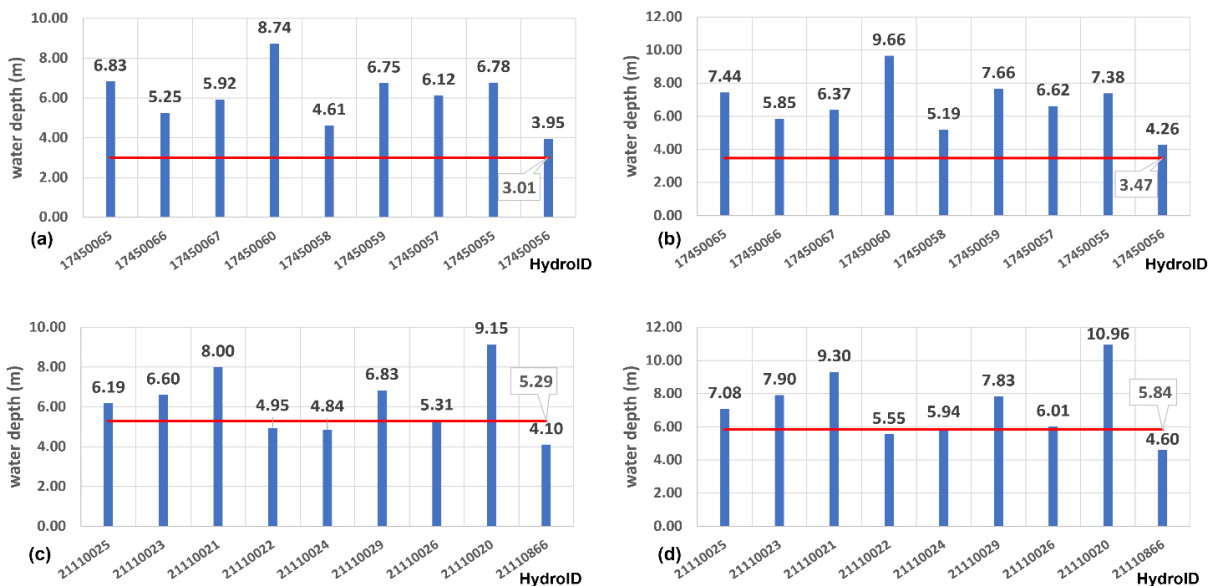
Figure 9. The depth estimates from the synthetic rating curve (red horizontal line) and from each catchment in 100- (first column) and 500-year flood scenarios (second column) in Clarksville (first row) and Rock Valley (second row)

The HAND model is a 'static' inundation mapping technique, as opposed to models that rely on hydrodynamic simulations, such as the HEC-RAS model. As a result, it may fail to provide as reliable inundation extent predictions in areas where a single depth is not enough to reflect the situations in sub-areas. As illustrated in Figure 9 (a) and (b), the synthetic depths are too small compared to the depths in each catchment, therefore making the single value less representative of the inundation condition in general. However, D_S can produce favorable results in areas where synthetic situation is relatively consistent with conditions in catchments, such as Rock Valley. Furthermore, compared to multi-depth approaches, D_S requires significantly less data and computational efforts compared to multi-depth approaches even the multi-depth ones are already quite data parsimonious compared to many traditional flood modeling approaches.

We believe that an efficient flood response strategy could first benefit from a fast model, such as the single-depth HAND framework, that requires the least data but can accurately show where major inundation will happen in order to support mitigation and planning decisions (Carson *et al.* 2018, Teague *et al.* 2021). Then it can follow a refined model, such as the multi-depth HAND, to ensure the inundation extent prediction free from major mismatches to benefit the accurate evacuation (Alabbad *et al.* 2021) and protection of people and property. Traditional flood inundation models can still be used for long-term planning, damage assessment, and documentation for the flood characteristics (such as inundation extent, localized maximum volume & stage), and serve as a reference to validate and improve data-driven flood models.

4.3. Performance of WBH with Different Model Configurations

For the 50-year flooding scenario in Rock Valley, Figure 10 depicts the WBH model performance among 31 threshold values and four water depth calculation approaches. As illustrated in Figure 10, the pattern of performance variation does not differ significantly between D_S, D_A, D_L, and D_{Local}. The B index is high when the threshold of 1% of total study area is used, indicating that the scene is overestimated. As the threshold increases, B and H decrease while PC, K, and F rise, indicating that the performance becomes balanced in terms of the number of overestimations and underestimations. Some indexes experience abrupt changes at two points. The first is at 2%, while the second is at 4%. After the 8% threshold for the total calculation area is exceeded, the performance becomes stable. For scenarios with D_S, D_A, and D_L approaches, the stable performance results are slightly overestimated (B value greater than 1) with PC and H values close to each other. Whereas the inundation extent is moderately underestimated for scenarios with D_{Local}.

Figure 11 depicts the bar charts with grouped indexes for the 8% of the study area after which the model performance becomes steady. As shown in Figure 11 (a), all the indexes are similar among the configurations utilizing D_A, D_L, and D_S except for H, which has a slightly larger value with D_L. The model configuration with D_{Local} produces the lowest performance for the 100-year flood, with lower values for all indexes. The patterns for F, K, and PC are the same for the 500-year scenario presented in Figure 11 (b), as the value using D_A is the largest, followed by D_S and then D_{Local}, and finally the value using D_L. For B and H, the greatest value comes from the D_L configuration, followed by comparative values from D_A and D_{Local} cases, and finally the one using D_S. As B and H increase with the increase of positive predictions, a high

value of B and H indicates the case using D_L generates more overestimation compared to the other three approaches.
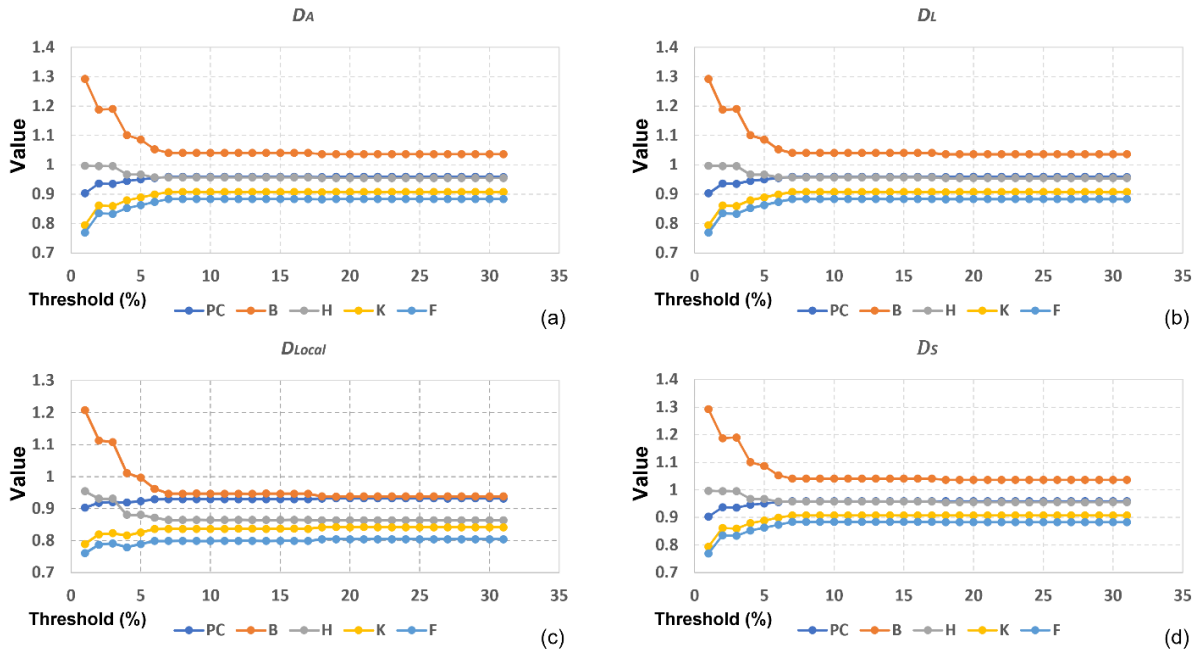
Figure 10. Comparing the model performance in Rock Valley with four depth calculation approaches in the 50-year flood scenario
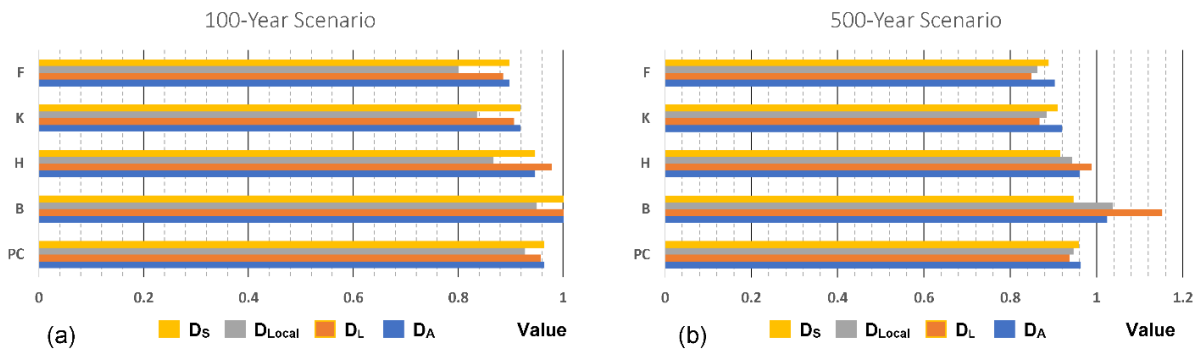
Figure 11. Comparing the stable performance of WBH at a fixed threshold of 8% for Rock Valley in 100-year and 500-year flood scenarios

Figure 12 shows model performance variation for Clarksville in the 50-year flooding event. There are two major changes for the model performance line among all thresholds tested. The two changes occur when the thresholds are about 6 and 12% of the study area, corresponding to the amount of 8.7 and 17.41 km². The 6 and 12% thresholds have made the performance curves stage-like where the performances are similar to each other within the same stage. Figure 13 shows the summarizing bar charts of grouped indexes with the four water depths and a drainage threshold of 12% of the study area for the 100- and 500-year flooding scenarios in Clarksville.

Figure 13 shows that the performance with D_A and D_L approaches are similar, followed by the configuration with D_{Local}, while D_S leads to the worst matching case for Clarksville in both

flooding scenarios. Also, all configurations except for the ones with D_S show overestimated inundation extent in general, whereas the B index for the case with D_S is about 0.7 in both flooding scenarios indicating there are major underestimations in the prediction.
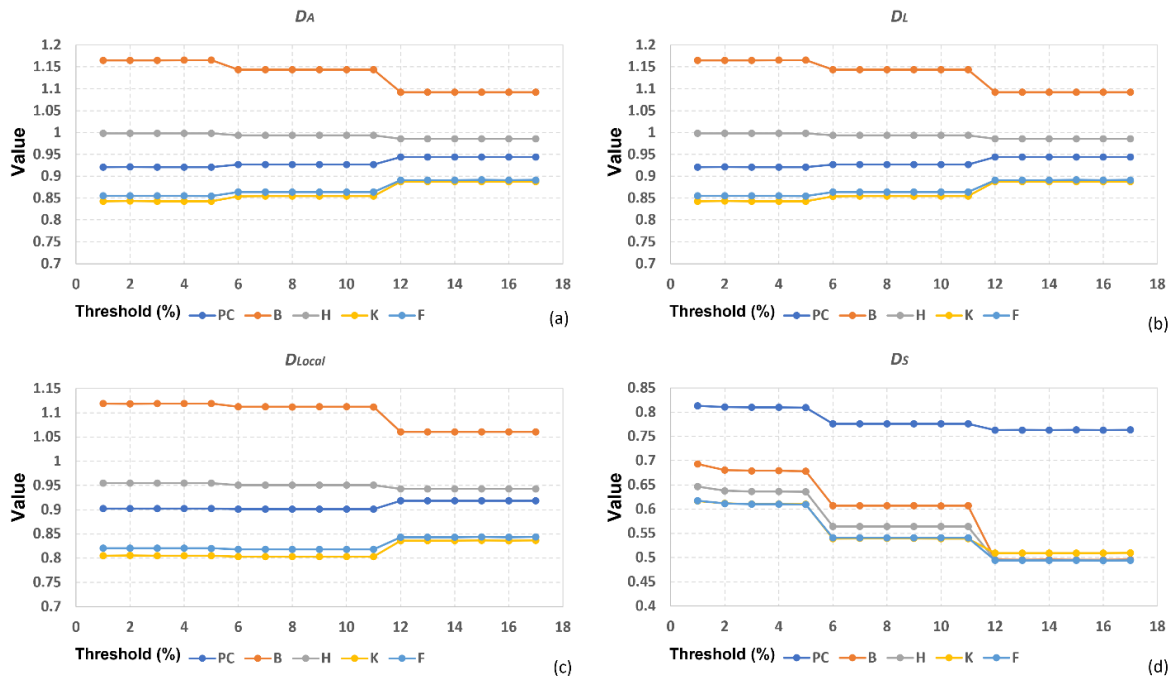
Figure 12. Model performance in Clarksville with four depth calculation approaches in the 50-year flood scenario
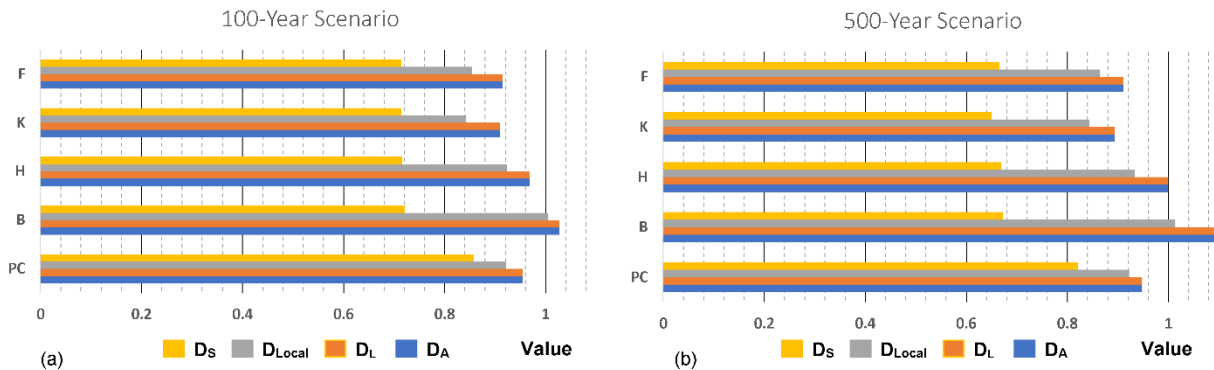
Figure 13. Comparing the stable performance of WBH at a fixed drainage threshold of 12% for Clarksville in 100-year and 500-year flood scenarios

Comparing Figure 10 results with Figure 12 we see that the major changes in model performance for Rock Valley occur between the drainage thresholds of 1% to 5 %, whereas it occurs between 5% to 12 % for Clarksville. For Rock Valley, all configurations generate a slightly overestimated inundation extent when the performance becomes stable except for the ones with D_{Local}. In addition, the overall performance increases as the drainage threshold increases until it reaches the threshold of about 8 %. For Clarksville, D_S failed to catch as many inundated pixels indicated on the reference map compared to the other three techniques. The extent is underestimated even with a 1% drainage threshold which corresponds to 1.45 km^2 which is the smallest threshold tested. Therefore, as the threshold increases, it brings more

underestimations and lowers the model performance. The performance with the multi-depth approaches, by contrast, is more accurate and resistant to underestimation.

Given the performance comparison, we think that D_A and D_L outperform D_{Local} not only because these three generate comparable results but also because D_{Local} necessitates additional computation to determine the areas that each catchment outlet drains so that varied water depths can be applied to the appropriate locations. The D_{Local} and NWCH computations differ in that the FIM 3 versions consider flooding in each impacted catchment separately as water is not allowed to spread beyond the catchment boundary. The scope of each catchment is recorded in a GeoPackage file that is not usually updated. By contrast, in D_{Local}, the region each outlet drains is defined by flow directions, which means that the area an outlet controls varies depending on the thresholds and DEM inputs. Therefore, D_{Local} provides a more accurate representation of possible changes to the topography (such as dredging and land cover changes) and provides users of the system with greater flexibility.

Previous research has demonstrated that a drainage threshold of 4 km^2 reduces mismatches and improves inundation extent forecasts (Nobre *et al.* 2016). However, the findings of this study reveal that the 4 km^2 does not produce the best results in either study region since it is too small and leads to overestimation. Our findings also reveal that the first turning point for performance occurs approximately around 5 to 6% of the area, but there may be another value after which the performance can improve further, as shown in Clarksville.

4.4. Impact of Bathymetry Information on Model Performance

Figure 14 shows the elevation difference in the river channels for Clarksville and Rock Valley between the bathymetry measurements and raw Lidar-based DEM. As mentioned earlier, the bathymetry measurements are only available in the river channels. The elevation differences are -0.608±1.01 m, and -1.210±0.4 m between the bathymetry measurements and the raw DEM in Rock Valley and Clarksville, respectively. We noticed that there are some pixels with extremes values in both study areas shown in Figure 14. In addition to measuring errors, they may also be attributable to the inconsistency and changes happened between the time the two products were made available. The DEM is created using mostly the Lidar measurements between 2007 to 2009, while the bathymetry data were collected between 2013 and 2014. Figure 15 shows the performance variation with D_A in the 100-year flooding scenario for Rock Valley and in the 500-year flooding scenario for Clarksville before and after the bathymetry measurements are added.
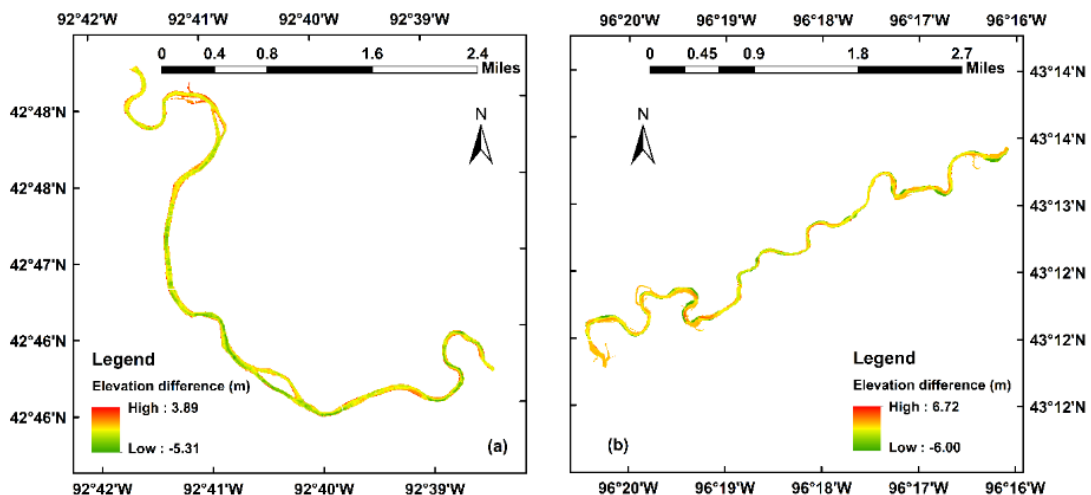
Figure 14. Elevation difference between the bathymetry measurements and the raw DEM for Clarksville (a) and Rock Valley (b)

(a)

(b)

(c)

(d)
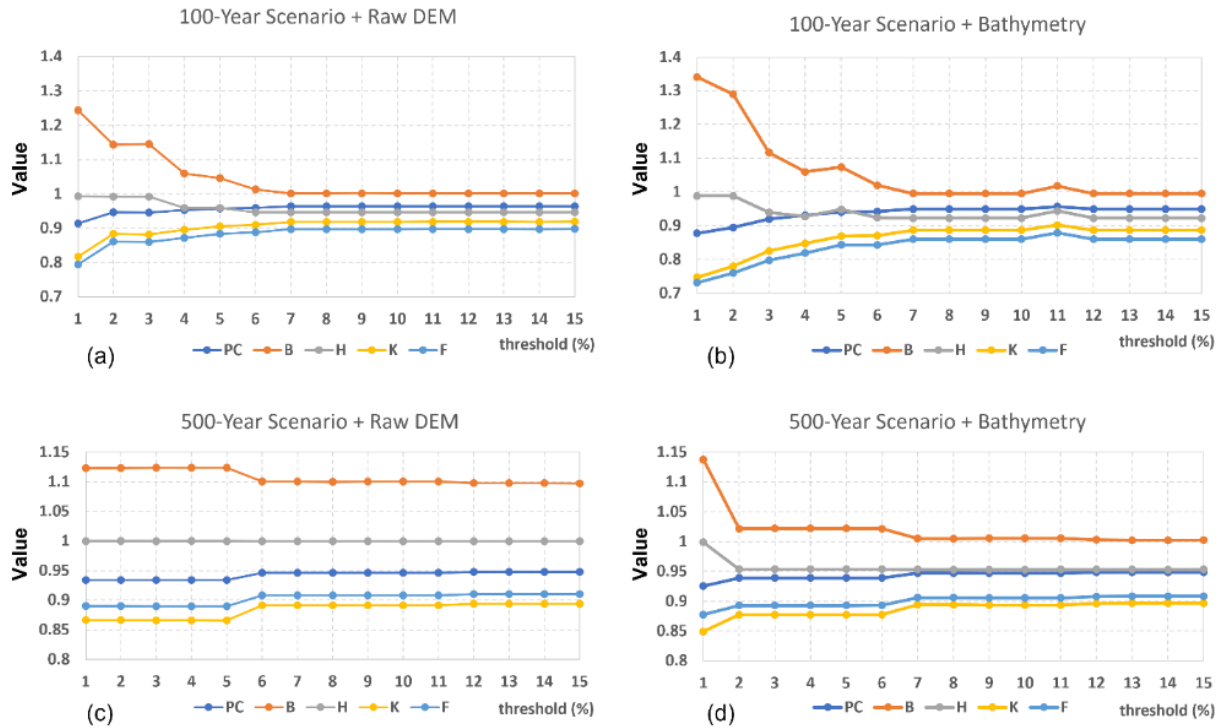
Figure 15. Comparing the performance before (first column) and after the bathymetry data added (second column) for Rock Valley (first row) and Clarksville (second row)

When comparing Figure 15 (a) and (b), it is obvious that the bathymetry causes some variation in model performance, such as the cases with the thresholds of 2, 3, 5, and 11% while the overall trend remains the same. It is also observed that adding bathymetry measurements increased overestimates significantly for cases with low thresholds. After the 8% threshold, performance with bathymetry data becomes stable, similar to performance with raw DEM. Furthermore, the steady performance demonstrated in Figure 15 (a) and (b) is comparable but slightly lower than cases without bathymetry. Similarly, the setup with a 1% threshold with bathymetry information in Clarksville is slightly worse as it produces more overestimation.

Table 3. Comparing model performance with and without the bathymetry measurements for the two study areas for which all cases have a drainage threshold of 8 % of the total area. For each pair sharing the same water depth computation approach, the upper row is the one with the raw DEM and the lower one is that with bathymetry information.

	Return Period	Depth	TP	FN	FP	TN	FP+FN	PC	B	H	K	F
Clarksville	500-year	D_A	86564	34	8703	67082	8737	0.946	1.100	1.000	0.891	0.908
			82541	4057	4492	71293	8549	0.947	1.005	0.953	0.894	0.906
		D_L	86564	34	8703	67082	8737	0.946	1.100	1.000	0.891	0.908
			85884	714	9526	66259	10240	0.937	1.102	0.992	0.872	0.893
		D_{Local}	80846	5752	7117	68668	12869	0.921	1.016	0.934	0.841	0.863

			73185	13413	3610	72175	17023	0.895	0.887	0.845	0.791	0.811
		D_S	65604	20994	811	74974	21805	0.866	0.767	0.758	0.735	0.751
			48487	38111	1178	74607	39289	0.758	0.574	0.560	0.528	0.552
Rock Valley	100-year	D_A	82406	4632	4756	166510	9388	0.964	1.001	0.947	0.919	0.898
			80301	6737	6329	164937	13066	0.949	0.995	0.923	0.887	0.860
		D_L	85207	1831	9152	162114	10983	0.957	1.084	0.979	0.907	0.886
			80301	6737	6329	164937	13066	0.949	0.995	0.923	0.887	0.860
		D_{Local}	75507	11531	7208	164058	18739	0.927	0.950	0.868	0.836	0.801
			72161	14877	5327	165939	20204	0.922	0.890	0.829	0.820	0.781
		D_S	82406	4632	4756	166510	9388	0.964	1.001	0.947	0.919	0.898
			80301	6737	6329	164937	13066	0.949	0.995	0.923	0.887	0.860

As indicated in Table 3, the B index decreased for almost all above cases when bathymetry data was taken into account, with the exception of the one in Clarksville with D_L. When compared to raw DEM data, the performance with bathymetry is marginally lower in all circumstances. Figures 16 and 17 depict a graphical comparison of the extent of inundation using D_A and D_{Local} for two areas with and without bathymetry data.
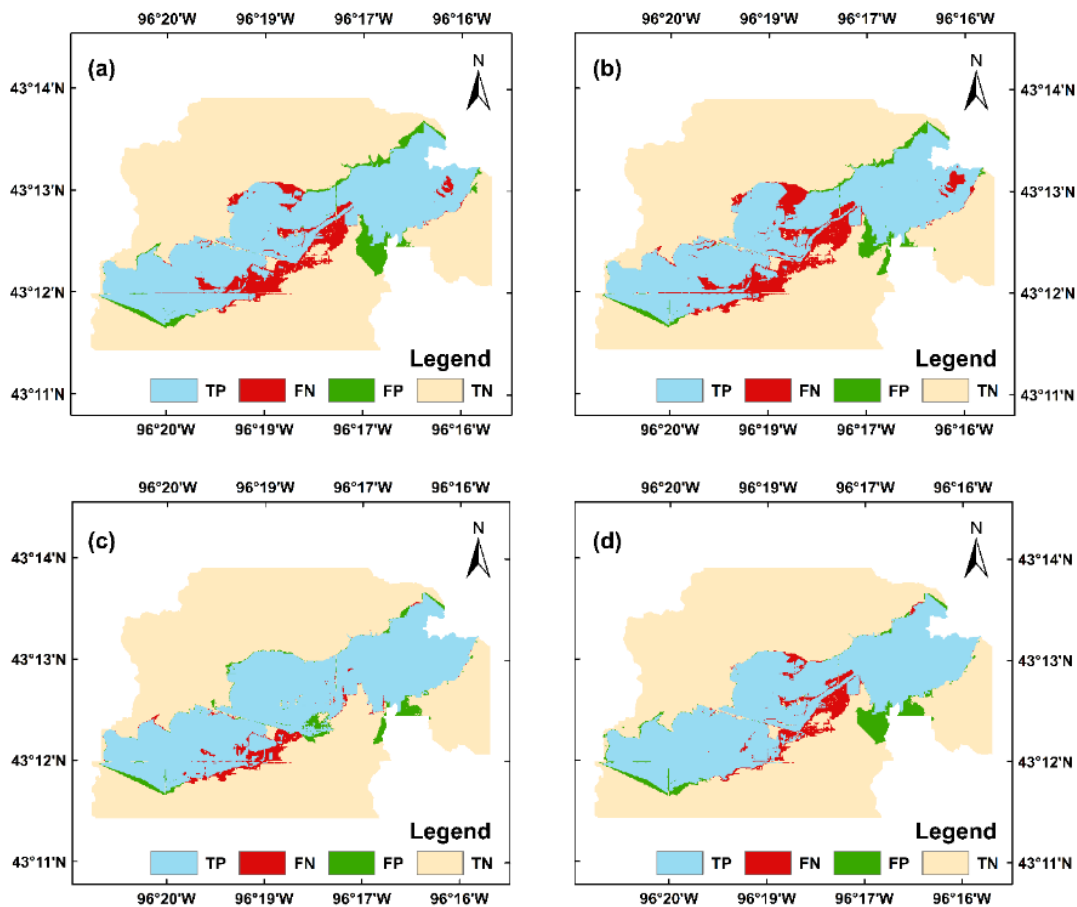
Figure 16. The inundation extent in Clarksville with the D_{Local} (first row) and D_A (second row) approaches using the raw DEM (first column) and the bathymetry measurements (second column) in the 500-year flooding scenario with a drainage threshold of 8% of the area

Figures 16 and 17 illustrate that, as compared to the raw DEM, inundation extent using bathymetry data shows slightly higher underestimation. The HAND value, as mentioned in previous sections, is the elevation difference between any non-stream pixel and the stream pixel to which it drains. As a result, as the elevation of stream points decreases, the HAND value of non-stream points increases. This can result in a more balanced outcome for some cases as the ones shown by Table 3 using D_A and D_L in Clarksville and Rock Valley as they have a smaller B index with the bathymetry information. However, it can worsen the underestimation the extent is already underestimated as shown in the situations of D_S in Clarksville and D_{Local} in Rock Valley. We also noticed a slightly lower performance for those with inundation condition changed from overestimation to underestimation (cases with D_{Local} in Clarksville and all cases except for the those with D_{Local} in Rock Valley).
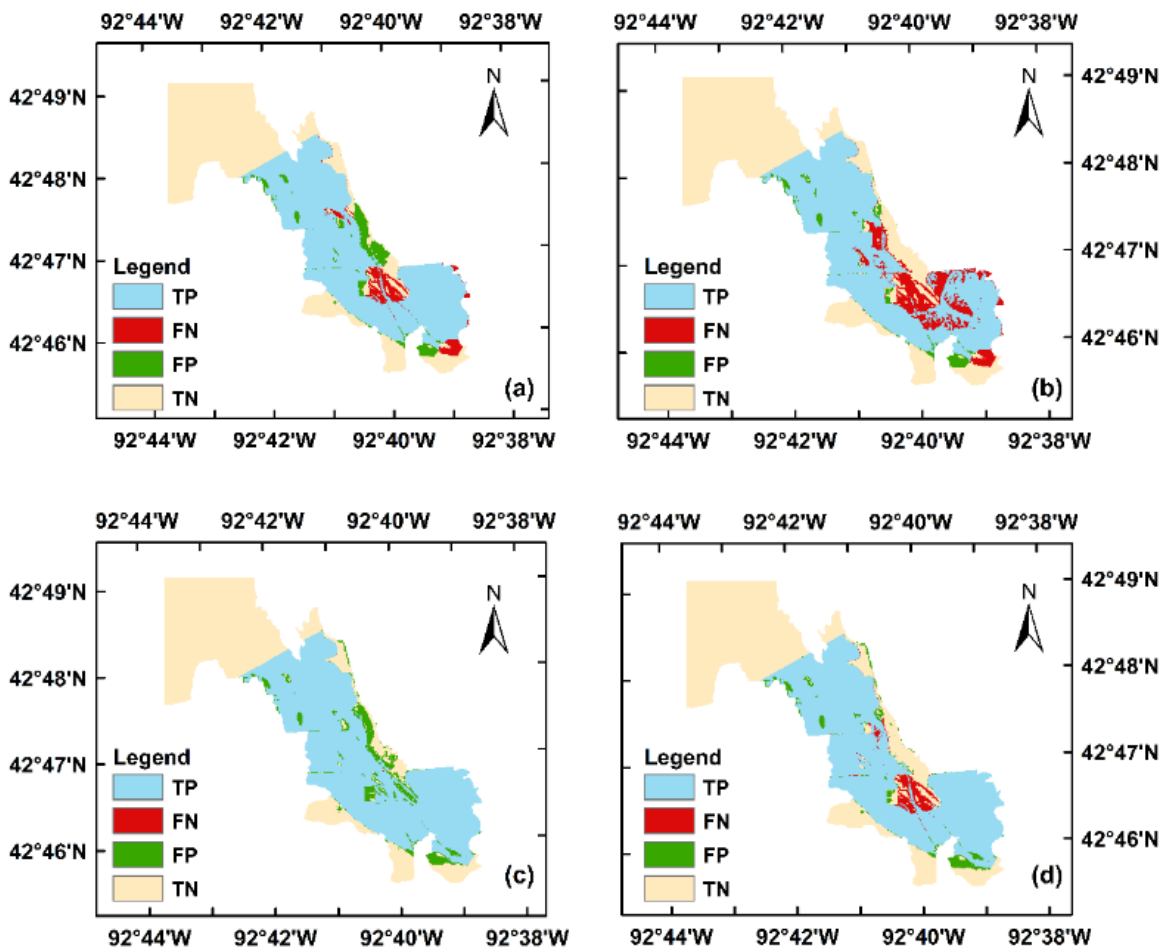
Figure 17. The inundation extent in Rock Valley with the D_{Local} (first row) and D_A (second row) approaches using the raw DEM (first column) and the bathymetry measurements (second column) in the 100-year flooding scenario with a drainage threshold of 8 % of the area

Although False-Positive results could cause wasting resources and labor during flood hazard prevention, False-Negative predictions are more dangerous as it may lead to insufficient preparation that will increase economic losses and casualties. Therefore, we believe that the bathymetry data should be treated with care.

Conclusion

In this study, we first examined the performance of a rating-curve-based (NWCH) and a non-rating-curve-based (WBH) technique to generate flood inundation maps based on HAND. The former was represented by a framework built by the National Water Center, while the latter was integrated into a web-based system, which provides greater flexibility in terms of data needs and computation techniques. The results show that the WBH with the least data input (a single water depth value, an unadjusted drainage threshold, and DEM) can generate comparable inundation extent predictions to the NWCH in areas where the synthetical and catchment situations are relatively consistent. Otherwise, WBH predictions with the simplest model configuration may be underestimated due to a combination of 1) localized flow direction changes caused by the pit-removing algorithm; 2) inaccuracy of the HAND values at a pixel level due to data format transformation and storage; and 3) differences between the depth estimates for the synthetic region and those for each catchment. Underestimation can be avoided by employing multiple water depths rather than just using one.

We also tested the performance of HAND with various model configurations for WBH model. Our results indicate that using 4 km^2 as the drainage threshold value as suggested by early studies results in too many overestimations in both study areas. In our cases, a good threshold falls in the range of 8 to 12 % of the total area after which the model performance becomes stable. We did not see significant performance differences among cases with the three multi-depth approaches (D_A, D_L, and D_{Local}) as no approach can consistently outperform the others considering different flooding scenarios and study areas. We, therefore, believe that D_A and D_L are better than D_{Local} as they require less computation effort. Besides that, all three multi-depth approaches are more robust to factors that may lead to underestimation as compared with D_S.

Finally, our tests indicate that more underestimations will occur with the bathymetry data added. This is because the HAND values for non-drainage pixels will increase due to decreased elevation for drainage pixels. The increased underestimation could help achieve a more balanced prediction if the region is overestimated previously but can also make the performance worse if the original one is already underestimated. We believe that the bathymetry data should be treated with care as underestimation is usually more dangerous than overestimation in flood extent predictions since the former will put under-prepared communities and properties at risk. Our study demonstrated the efficiency and usefulness of the client-side, real-time web-based flood mapping system designed with non-rating-curve-based HAND and provided in-depth analyses of the HAND model which can serve as general guidelines for model setup and performance improvement.

Reference

Abdrabo, K.I., Kantosh, S.A., Saber, M., Sumi, T., Elleithy, D., Habiba, O.M., and Alboshy, B., 2022. The Role of Urban Planning and Landscape Tools Concerning Flash Flood Risk Reduction Within Arid and Semiarid Regions. *In*: *Wadi Flash Floods*. 283–316.

Afshari, S., Tavakoly, A.A., Rajib, M.A., Zheng, X., Follum, M.L., Omranian, E., and Fekete, B.M., 2018. Comparison of new generation low-complexity flood inundation mapping tools with a hydrodynamic model. *Journal of Hydrology*, 556, 539–556.

Agliamzanov, R., Sit, M., and Demir, I., 2020. Hydrology@Home: a distributed volunteer computing framework for hydrological research and applications. *Journal of Hydroinformatics*, 22 (2), 235–248.

Alabbad, Y., Mount, J., Campbell, A.M., and Demir, I., 2021. Assessment of transportation system disruption and accessibility to critical amenities during flooding: Iowa case study. *Science of The Total Environment*, 793, 148476.

Alabbad, Y., Yildirim, E., and Demir, I., 2022. Flood mitigation data analytics and decision support framework: Iowa Middle Cedar Watershed case study. *Science of The Total Environment*, 814, 152768.

Di Baldassarre, G., Saccà, S., Aronica, G.T., Grimaldi, S., Ciullo, A., and Crisci, M., 2017. Human-flood interactions in Rome over the past 150 years. *Advances in Geosciences*, 44, 9–13.

Baldassarre, G.D., Nardi, F., Annis, A., Odongo, V., Rusca, M., and Grimaldi, S., 2020. Brief communication: Comparing hydrological and hydrogeomorphic paradigms for global flood hazard mapping. *Natural Hazards and Earth System Sciences*, 20 (5), 1415–1419.

Barnes, R., Lehman, C., and Mulla, D., 2014. An efficient assignment of drainage direction over flat surfaces in raster digital elevation models. *Computers and Geosciences*, 62, 128–135.

Bentivenga, M., Giano, S.I., and Piccarreta, M., 2020. Recent Increase of Flood Frequency in the Ionian Belt of Basilicata Region, Southern Italy: Human or Climatic Changes? *Water 2020, Vol. 12, Page 2062*, 12 (7), 2062.

Blöschl, G., Kiss, A., Viglione, A., Barriendos, M., Böhm, O., Brázdil, R., Coeur, D., Demarée, G., Llasat, M.C., Macdonald, N., Retsö, D., Roald, L., Schmocker-Fackel, P., Amorim, I., Bělínová, M., Benito, G., Bertolin, C., Camuffo, D., Cornel, D., Doktor, R., Elleder, L., Enzi, S., Garcia, J.C., Glaser, R., Hall, J., Haslinger, K., Hofstätter, M., Komma, J., Limanówka, D., Lun, D., Panin, A., Parajka, J., Petrić, H., Rodrigo, F.S., Rohr, C., Schönbein, J., Schulte, L., Silva, L.P., Toonen, W.H.J., Valent, P., Waser, J., and Wetter, O., 2020. Current European flood-rich period exceptional compared with past 500 years. *Nature 2020 583:7817*, 583 (7817), 560–566.

Carson, A., Windsor, M., Hill, H., Haigh, T., Wall, N., Smith, J., Olsen, R., Bathke, D., Demir, I., and Muste, M., 2018. Serious gaming for participatory planning of multi-hazard mitigation. *International Journal of River Basin Management*, 16 (3), 379–391.

Demiray, B.Z., Sit, M., and Demir, I., 2021. D-SRGAN: DEM Super-Resolution with Generative Adversarial Networks. *SN Computer Science*, 2 (1), 1–11.

Ebert-Uphoff, I., Thompson, D.R., Demir, I., Gel, Y.R., Hill, M.C., Karpatne, A., Guereque, M., Kumar, V., Cabral-Cano, E., and Smyth, P., 2017. A vision for the development of benchmarks to bridge geoscience and data science. *In*: *7th International Workshop on Climate Informatics*.

Ewing, G. and Demir, I., 2021. An ethical decision-making framework with serious gaming: a smart water case study on flooding. *Journal of Hydroinformatics*, 23 (3), 466–482.

Garrote, J., González-Jiménez, M., Guardiola-Albert, C., and Díez-Herrero, A., 2021. The manning's roughness coefficient calibration method to improve flood hazard analysis in the absence of river bathymetric data: Application to the urban historical zamora city centre in spain. *Applied Sciences (Switzerland)*, 11 (19), 9267.

Ghosh, A. and Kar, S.K., 2018. Application of analytical hierarchy process (AHP) for flood risk assessment: a case study in Malda district of West Bengal, India. *Natural Hazards*, 94 (1), 349–368.

Gilles, D., Young, N., Schroeder, H., Piotrowski, J., and Chang, Y.J., 2012. Inundation mapping initiatives of the iowa flood center: Statewide coverage and detailed urban flooding analysis. *Water*

(Switzerland), 4 (1), 85–106.

Godbout, L., Zheng, J.Y., Dey, S., Eyelade, D., Maidment, D., and Passalacqua, P., 2019. Error Assessment for Height Above the Nearest Drainage Inundation Mapping. *Journal of the American Water Resources Association*, 55 (4), 952–963.

Haltas, I., Yildirim, E., Oztas, F., and Demir, I., 2021. A comprehensive flood event specification and inventory: 1930–2020 Turkey case study. *International Journal of Disaster Risk Reduction*, 56.

Hu, A. and Demir, I., 2021. Real-time flood mapping on client-side web systems using hand model. *Hydrology*, 8 (2), 65.

Jafarzadegan, K. and Merwade, V., 2019. Probabilistic floodplain mapping using HAND-based statistical approach. *Geomorphology*, 324, 48–61.

Janizadeh, S., Chandra Pal, S., Saha, A., Chowdhuri, I., Ahmadi, K., Mirzaei, S., Mosavi, A.H., and Tiefenbacher, J.P., 2021. Mapping the spatial and temporal variability of flood hazard affected by climate and land-use changes in the future. *Journal of Environmental Management*, 298, 113551.

Juurlink, D.N. and Detsky, A.S., 2005. Kappa statistic. *CMAJ*, 173 (1), 16–16.

Lancia, M., Zheng, C., He, X., Lerner, D.N., Andrews, C., and Tian, Y., 2020. Hydrogeological constraints and opportunities for "Sponge City" development: Shenzhen, southern China. *Journal of Hydrology: Regional Studies*, 28, 100679.

de Lange, J., 2019. 3. History of flood defenses in the Low Countries. *In*: *Security of Flood Defenses*. De Gruyter, 21–33.

Le, T. and Bae, D.H., 2020. Response of global evaporation to major climate modes in historical and future Coupled Model Intercomparison Project Phase 5 simulations. *Hydrology and Earth System Sciences*, 24 (3), 1131–1143.

Leitner, M., Babcicky, P., Schinko, T., and Glas, N., 2020. The status of climate risk management in Austria. Assessing the governance landscape and proposing ways forward for comprehensively managing flood and drought risk. *Climate Risk Management*, 30, 100246.

Li, Z. and Demir, I., 2022. A comprehensive web-based system for flood inundation map generation and comparative analysis based on height above nearest drainage. *Science of The Total Environment*, 828, 154420.

Li, Z., Mount, J., and Demir, I., 2022. Accounting for uncertainty in real-time flood inundation mapping using HAND model: Iowa case study. *Natural Hazards*, 1–28.

Liu, Y.Y., Maidment, D.R., Tarboton, D.G., Zheng, X., and Wang, S., 2018. A CyberGIS Integration and Computation Framework for High-Resolution Continental-Scale Flood Inundation Mapping. *JAWRA Journal of the American Water Resources Association*, 54 (4), 770–784.

Maidment, D.R., 2017. Conceptual Framework for the National Flood Interoperability Experiment. *JAWRA Journal of the American Water Resources Association*, 53 (2), 245–257.

Mark, D.M., 1984. Automated detection of drainage networks from digital elevation models. *Cartographica: The International Journal for Geographic Information and Geovisualization,* 21 (2–3), 168–178.

McGrath, H., Bourgon, J.F., Proulx-Bourque, J.S., Nastev, M., and Abo El Ezz, A., 2018. A comparison of simplified conceptual models for rapid web-based flood inundation mapping. *Natural Hazards*, 93 (2), 905–920.

Michael Johnson, J., Munasinghe, D., Eyelade, D., and Cohen, S., 2019. An integrated evaluation of the National Water Model (NWM)-Height above nearest drainage (HAND) flood mapping methodology. *Natural Hazards and Earth System Sciences*, 19 (11), 2405–2420.

Munoz, S.E., Giosan, L., Therrell, M.D., Remo, J.W.F., Shen, Z., Sullivan, R.M., Wiman, C., O'Donnell, M., and Donnelly, J.P., 2018. Climatic control of Mississippi River flood hazard amplified by river engineering. *Nature 2018 556:7699*, 556 (7699), 95–98.

Musser, J., Watson, K., Painter, J., and Gotvald, A., 2016. Flood-inundation maps of selected areas affected by the flood of October 2015 in central and coastal South Carolina.

Nardi, F., Annis, A., Baldassarre, G. Di, Vivoni, E.R., and Grimaldi, S., 2019. GFPLAIN250m, a global high-resolution dataset of earth's floodplains. *Scientific Data*, 6 (1), 1–6.

Nicholls, R.J., Lincke, D., Hinkel, J., Brown, S., Vafeidis, A.T., Meyssignac, B., Hanson, S.E., Merkens, J.L., and Fang, J., 2021. A global analysis of subsidence, relative sea-level change and coastal flood exposure. *Nature Climate Change 2021 11:4*, 11 (4), 338–342.

NOAA, 2021. NOAA-OWP/cahaba: Flood inundation mapping and evaluation software configured to work with U.S. National Water Model. [online]. Available from: https://github.com/NOAA-OWP/cahaba [Accessed 30 Dec 2021].

Nobre, A.D., Cuartas, L.A., Hodnett, M., Rennó, C.D., Rodrigues, G., Silveira, A., Waterloo, M., and Saleska, S., 2011. Height Above the Nearest Drainage - a hydrologically relevant new terrain model. *Journal of Hydrology*, 404 (1–2), 13–29.

Nobre, A.D., Cuartas, L.A., Momo, M.R., Severo, D.L., Pinheiro, A., and Nobre, C.A., 2016. HAND contour: A new proxy predictor of inundation extent. *Hydrological Processes*, 30 (2), 320–333.

Nohani, E., 2019. Estimating the Manning's Roughness Coefficient in Rivers by Experimental Method. *Foot*, 1 (6), 50.

Papaioannou, G., Vasiliades, L., Loukas, A., and Aronica, G.T., 2017. Probabilistic flood inundation mapping at ungauged streams due to roughness coefficient uncertainty in hydraulic modelling. *Advances in Geosciences*, 44, 23–34.

Provost, F., 1998. Glossary of Terms Special Issue on Applications of Machine Learning and the Knowledge Discovery Process. *Machine Learning*, 30, 271–274.

Psomiadis, E., Tomanis, L., Kavvadias, A., Soulis, K.X., Charizopoulos, N., and Michas, S., 2021. Potential Dam Breach Analysis and Flood Wave Risk Assessment Using HEC-RAS and Remote Sensing Data: A Multicriteria Approach. *Water 2021, Vol. 13, Page 364*, 13 (3), 364.

Rebolho, C., Andréassian, V., and Le Moine, N., 2018. Inundation mapping based on reach-scale effective geometry. *Hydrology and Earth System Sciences*, 22 (11), 5967–5985.

Rennó, C.D., Nobre, A.D., Cuartas, L.A., Soares, J.V., Hodnett, M.G., Tomasella, J., and Waterloo, M.J., 2008. HAND, a new terrain descriptor using SRTM-DEM: Mapping terra-firme rainforest environments in Amazonia. *Remote Sensing of Environment*, 112 (9), 3469–3481.

S Chegwidden, O., Rupp, D.E., and Nijssen, B., 2020. Climate change alters flood magnitudes and mechanisms in climatically-diverse headwaters across the northwestern United States. *Environmental Research Letters*, 15 (9), 094048.

Savage, J.T.S., Bates, P., Freer, J., Neal, J., and Aronica, G., 2016. When does spatial resolution become spurious in probabilistic flood inundation predictions? *Hydrological Processes*, 30 (13), 2014–2032.

Seo, B.C., Keem, M., Hammond, R., Demir, I., and Krajewski, W.F., 2019. A pilot infrastructure for searching rainfall metadata and generating rainfall product using the big data of NEXRAD. *Environmental Modelling and Software*, 117, 69–75.

Shastry, A., Egbert, R., Aristizabal, F., Luo, C., Yu, C.-W., and Praskievicz, S., 2019. Using Steady-State Backwater Analysis to Predict Inundated Area from National Water Model Streamflow Simulations. *JAWRA Journal of the American Water Resources Association*, 55 (4), 940–951.

Sit, M., Langel, R.J., Thompson, D., Cwiertny, D.M., and Demir, I., 2021. Web-based data analytics framework for well forecasting and groundwater quality. *Science of The Total Environment*, 761, 144121.

Sit, M., Sermet, Y., and Demir, I., 2019. Optimized watershed delineation library for server-side and client-side web applications. *Open Geospatial Data, Software and Standards*, 4 (1), 1–10.

Speckhann, G.A., Borges Chaffe, P.L., Fabris Goerl, R., Abreu, J.J. de, and Altamirano Flores, J.A., 2018. Flood hazard mapping in Southern Brazil: a combination of flow frequency analysis and the HAND model. *Hydrological Sciences Journal*, 63 (1), 87–100.

Sun, X., Zhang, H., Hua, D., and Wei, B., 2021. The Influence of Urbanization on Storm Runoff. *In*: *IOP Conference Series: Earth and Environmental Science*. IOP Publishing, 022031.

Tadesse, Y.B. and Fröhle, P., 2020. Modelling of flood inundation due to levee breaches: Sensitivity of flood inundation against breach process parameters. *Water (Switzerland)*, 12 (12), 3566.

Tarboton, D.G., 1997. A new method for the determination of flow directions and upslope areas in grid digital elevation models. *Water Resources Research*, 33 (2), 309–319.

Teague, A., Sermet, Y., Demir, I., and Muste, M., 2021. A collaborative serious game for water resources planning and hazard mitigation. *International Journal of Disaster Risk Reduction*, 53, 101977.

Teng, J., Jakeman, A.J., Vaze, J., Croke, B.F.W., Dutta, D., and Kim, S., 2017. Flood inundation modelling: A review of methods, recent advances and uncertainty analysis. *Environmental Modelling and Software*.

Terezinha, V., Boulomytis, G., Zuffo, A.C., Gilberto, J., Filho, D., Monzur, &, Imteaz, A., Carlos Zuffo, A., and Alam Imteaz, M., 2017. Estimation and calibration of Manning's roughness coefficients for ungauged watersheds on coastal floodplains. *http://dx.doi.org/10.1080/15715124.2017.1298605*, 15 (2), 199–206.

Wilks, D.S., 2011. *Statistical Methods in the Atmospheric Sciences*. Academic Press.

Xu, H., Demir, I., Koylu, C., and Muste, M., 2019. A web-based geovisual analytics platform for identifying potential contributors to culvert sedimentation. *Science of The Total Environment*, 692, 806–817.

Yildirim, E. and Demir, I., 2021. An Integrated Flood Risk Assessment and Mitigation Framework: A Case Study for Middle Cedar River Basin, Iowa, US. *International Journal of Disaster Risk Reduction*, 56, 102113.

Zheng, X., Tarboton, D.G., Maidment, D.R., Liu, Y.Y., and Passalacqua, P., 2018. River Channel Geometry and Rating Curve Estimation Using Height above the Nearest Drainage. *Journal of the American Water Resources Association*, 54 (4), 785–806.